Technical Report 1644
March 1994

Propagation in the Evaporation Duct

Model Predictions and Comparisons to Data

R. A. Paulus

NRaD

Technical Report 1644
March 1994

Propagation in the Evaporation Duct

Model Predictions and Comparisons to Data

R. A. Paulus

NAVAL COMMAND, CONTROL AND OCEAN SURVEILLANCE CENTER RDT&E DIVISION San Diego, California 92152–5001

K. E. EVANS, CAPT, USN
Commanding Officer

R. T. SHEARER
Executive Director

ADMINISTRATIVE INFORMATION

Work for this report was performed by members of the Tropospheric Branch, Code 543, in the Ocean and Atmospheric Sciences Division, Code 54, at the Naval Command, Control and Ocean Surveillance Center RDT&E Division, San Diego, California. 92152–5001.

The work was funded by the Office of Naval Research, 800 North Quincy Street, Code 322, Arlington, VA 22217.

Released by
R. A. Paulus, Head
Tropospheric Branch

Under authority of
J. H. Richter, Head
Ocean and Atmospheric
Sciences Division

RV

EXECUTIVE SUMMARY

OBJECTIVE

Statistically compare predictions and observations of propagation loss for L-, S-, X-, and Ku-band in evaporation ducting conditions.

RESULTS

1. A modified evaporation duct calculation was shown to have skill in improving point-by-point propagation predictions at all frequencies.

2. Atmospheric surface-layer stability effects did not make a significant difference in propagation loss predictions for the given data set.

3. Range-variation of the evaporation duct was shown to account for observed signal variations that had not been previously explained.

RECOMMENDATIONS

Current propagation models and relatively simple characterizations of the evaporation duct can be used to assess signal level variations.

CONTENTS

FIGURES

TABLES

INTRODUCTION

This report compares and analyzes propagation in the evaporation duct utilizing data that was obtained in the eastern Mediterranean in 1972 with current evaporation duct characterizations and propagation models.

BACKGROUND

In 1972, a series of radio propagation measurements in the 1- to 40-GHz frequency range was performed in the eastern Mediterranean (*Richter and Hitney*, 1988). A 35.2-km, over-the-horizon, propagation path was established between the islands of Naxos and Mykonos in the Aegean Sea. Measurements were conducted during four different periods: February, April, August, and November; in four radar frequency bands: L, S, X, and Ku; and at three different receiver altitudes. Routine meteorological data were available from the Greek Weather Service on Naxos. During the last period, November, a Ka-band transmitter and two receivers were added to the experiment, and a meteorological ground station was established by U.S. Navy laboratory personnel at the receiver site on Mykonos. Analysis of the data revealed that trends in duct height agreed with trends in the radio data. A quantitative analysis, of observed propagation loss with that predicted by a waveguide model for one of the X-band links and a subset of the meteorological data, yielded a correlation coefficient of 0.71.

Patterson (1985) used a subset of the Greek data in evaluating three evaporation duct and two propagation models. He found that the evaporation duct models function equally well, considering the statistical average of meteorological inputs, but point-observed meteorological data caused a wide variation in model output. Patterson also found reasonable agreement between model-predicted and observed mean propagation loss; however, there was considerable variance that he attributed, in part, to variance in the evaporation duct characterizations. *Paulus* (1985) proposed a technique to reduce the sensitivity of the evaporation duct calculations to spurious meteorological measurements. This technique was incorporated into the U.S. Navy's IREPS (*Hitney and Richter*, 1976) and was used to regenerate a climatological database of evaporation duct heights (*Anderson*, 1987). Subsequently, this database was used in statistical assessments of propagation in the evaporation duct and was found to show good agreement with measured data, particularly at median levels (*Hitney and Vieth*, 1990; *Hitney and Hitney*, 1990); however, there remained discrepancies at higher and lower propagation loss values that were thought to be due to propagation effects not modeled, such as surface-based ducts from elevated refractive layers, subrefractive layers, and range-varying refractive structure.

In this report, the November 1972 Greek data are re-analyzed with current evaporation duct characterizations and propagation models. The DATA AND MODELS section describes the radio-meteorological data and propagation models used. The DATA ANALYSIS section presents the analysis. The CONCLUSIONS section summarizes the findings.

DATA AND MODELS

METEOROLOGICAL DATA

The 15-day measurement period in November 1972 was selected for analysis because it was the only period that had meteorological measurements on both Mykonos and Naxos. On Mykonos, the air temperature, relative humidity, and wind speed data were extracted hourly from strip chart recordings of instruments at a meteorological ground station; seawater temperature was measured manually by taking a sample from the surf zone with a bucket (*Anderson and Hitney*, private communication). Data were collected from 1000 on the 7th of November to 0900 on the 21st (Eastern European Standard Time). The Greek Weather Service on Naxos was located a few kilometers from the coast, and it provided hourly air temperature and relative humidity, three-hourly wind speed and direction, and twice daily sea temperature. To have consistent sampling of the meteorological data at both sites, the Naxos wind and sea temperature data were linearly interpolated to hourly values. Figures 1 through 5 are the plots of meteorological data, showing temporal and spatial variation for both sites. These data were used to characterize the refractive structure of the atmospheric surface layer, the first few tens of meters of the atmosphere over the ocean.

RADIO DATA

Radio data were collected from 5 to 21 November, for five frequencies over the 35.2-km path. Table 1 lists the propagation link characteristics for four of the frequencies; the Ka-band frequency was not analyzed for this study. Additional description of the experimental setup is in *Richter and Hitney* (1988).

PROPAGATION MODELS

The propagation models used in this study were the Engineer's Refractive Effects Prediction System (EREPS) described by *Patterson et al.* (1990) and the Radio Physical Optics (RPO) model described by *Hitney* (1992).

The EREPS propagation models are the same as those of IREPS. In the case of evaporation duct propagation, the EREPS/IREPS models are height-gain curves fitted to waveguide model solutions for modified refractivity, M, profiles calculated for neutral stability conditions (air temperature $\approx$ sea temperature) and characterized by duct height. EREPS is organized in a manner that specifically allows for comparative studies. In this study, the EREPS program PROPR was used to generate propagation loss curves for each link in Table 1 parametrically in evaporation duct height in 1-m increments from 0 to 40 m. The resulting values of propagation loss versus evaporation duct height are shown in figures 6 through 9. A zero-m evaporation duct corresponds closely to propagation through a standard atmosphere. As evaporation duct height increases, propagation loss decreases in a manner that is frequency dependent. At some duct height, propagation loss may reach a minimum and begin to increase again for further increases in duct height. This indicates that the first mode is fully trapped and that multiple modes may now affect the propagation loss calculation; however, the EREPS propagation model uses only one mode of propagation for an evaporation duct and may be in error for certain duct height and frequency combinations. To picture the magnitude of these errors, the high antenna curve of figures 6 through 9 can be compared to figure 1 of *Hitney and Vieth* (1990) which was calculated from a waveguide model.

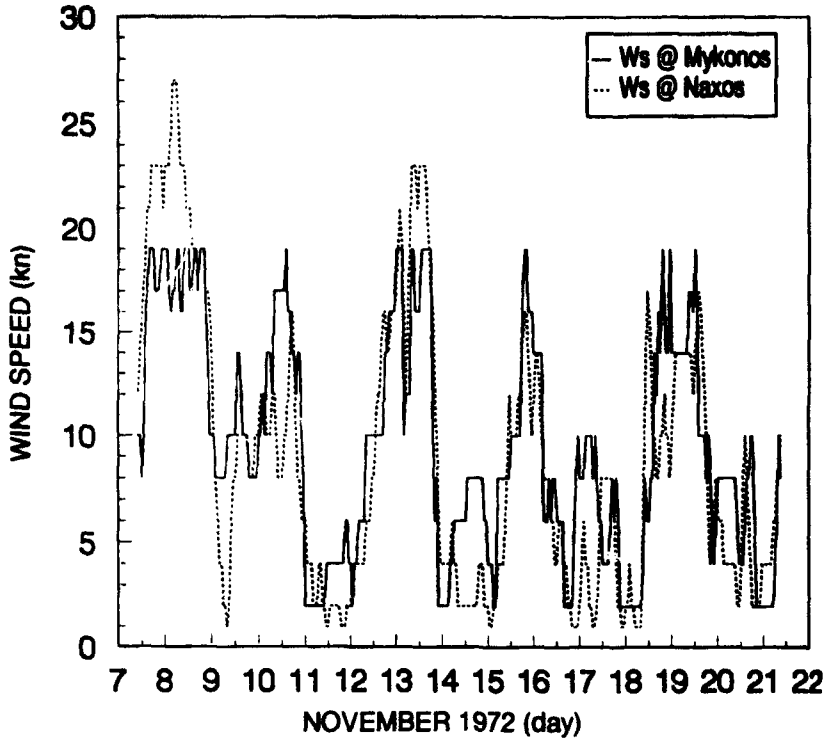

Figure 1. Wind speed, Ws, measured on the two islands.

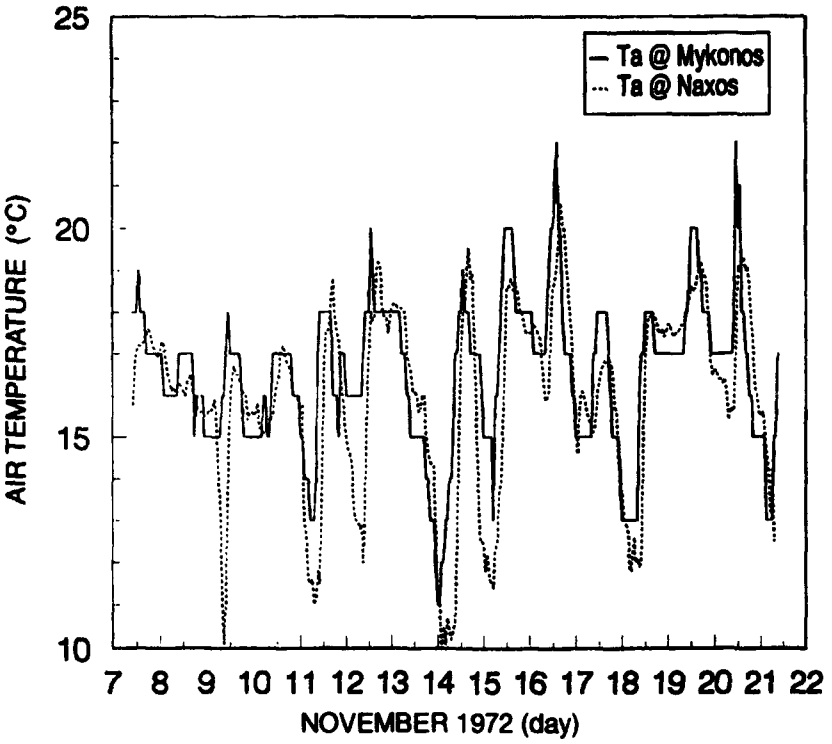

Figure 2. Air temperature, Ta, measured on the two islands.

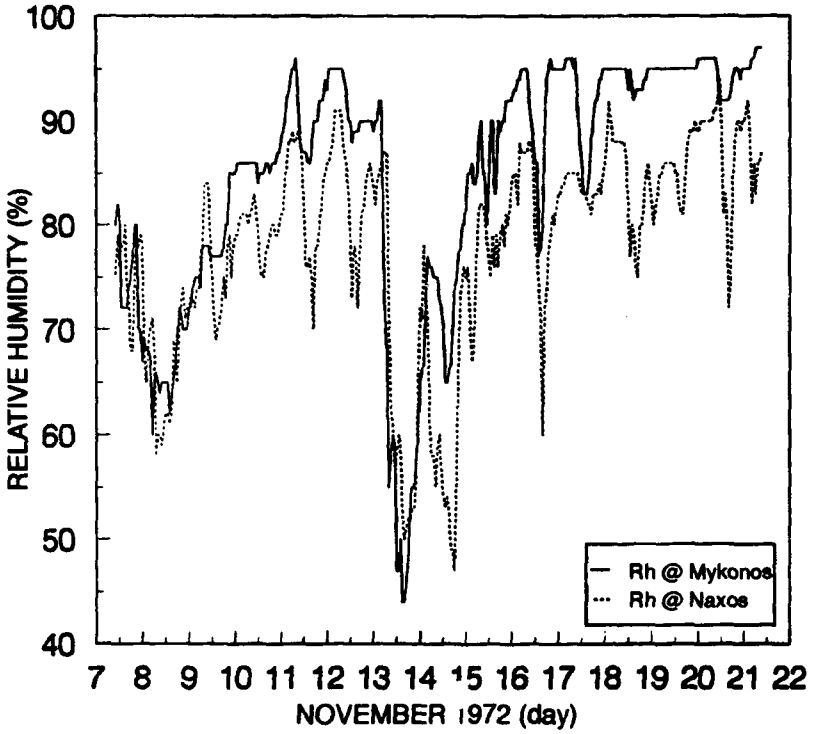

Figure 3. Relative humidity, Rh, measured on the two islands.

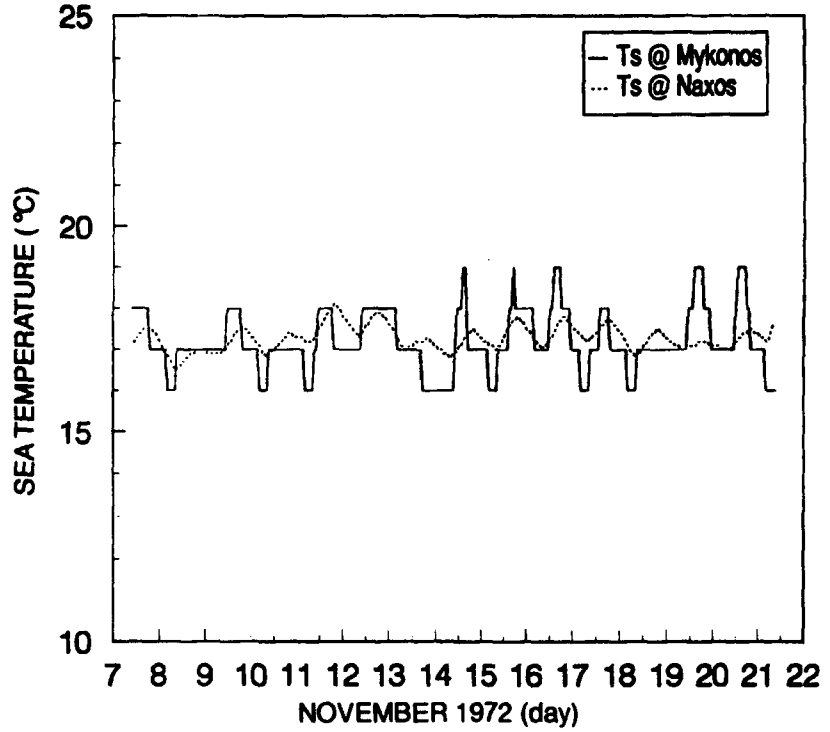

Figure 4. Sea temperature, Ts, measured on the two islands.

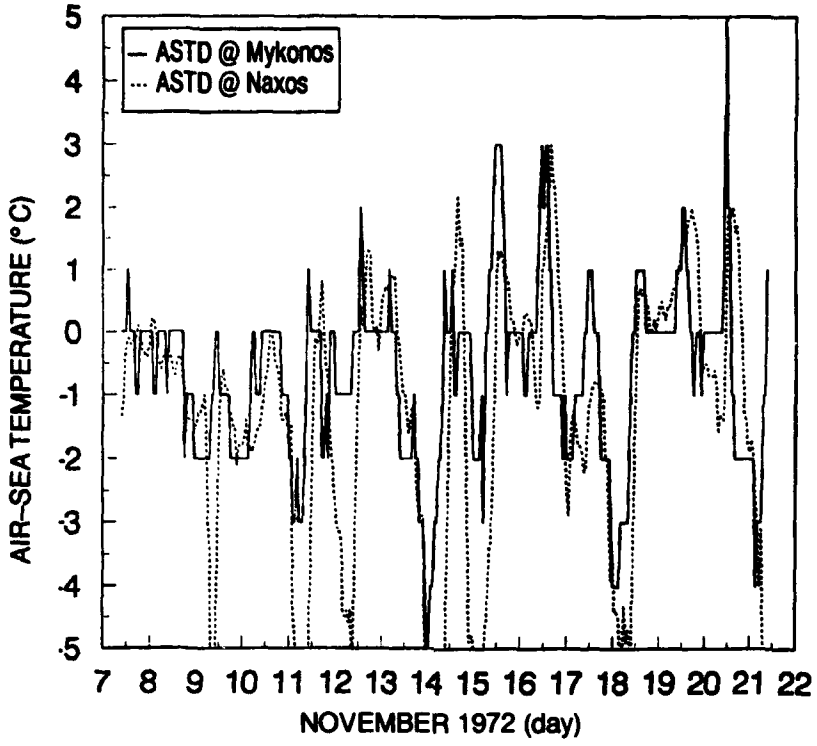

Figure 5. Air-sea temperature difference, ASTD, measured on the two islands.

Table 1. Propagation link characteristics for the November 1972 Greek islands experiment (*Richter and Hitney*, 1988).

PROPAGATION LINK CHARACTERISTICS					
Frequency Band		L	S	X	Ku
Transmitter Frequency (GHz)		1.0426	3.0075	9.624	17.9648
Transmitter antenna Height (m) (MSL)		4.8	4.8	4.8	4.5
Receiver antenna heights (m) MSL	High	19.2	19.2	19.2	17.8
	Mid	10.0	10.0	10.0	9.5
	Low	4.9	4.9	4.9	4.3

m = meters
MSL = mean sea level

RPO is a hybrid propagation model that uses a combination of ray optics and split-step parabolic equation methods to compute propagation loss. RPO requires a profile (or profiles) of modified refractivity as input as opposed to the profile characterization in terms of a single duct height used by EREPS. RPO was run in both the range-independent mode using one profile generated from the Mykonos meteorological data and the range-dependent mode using two profiles generated from Mykonos and Naxos meteorological data.

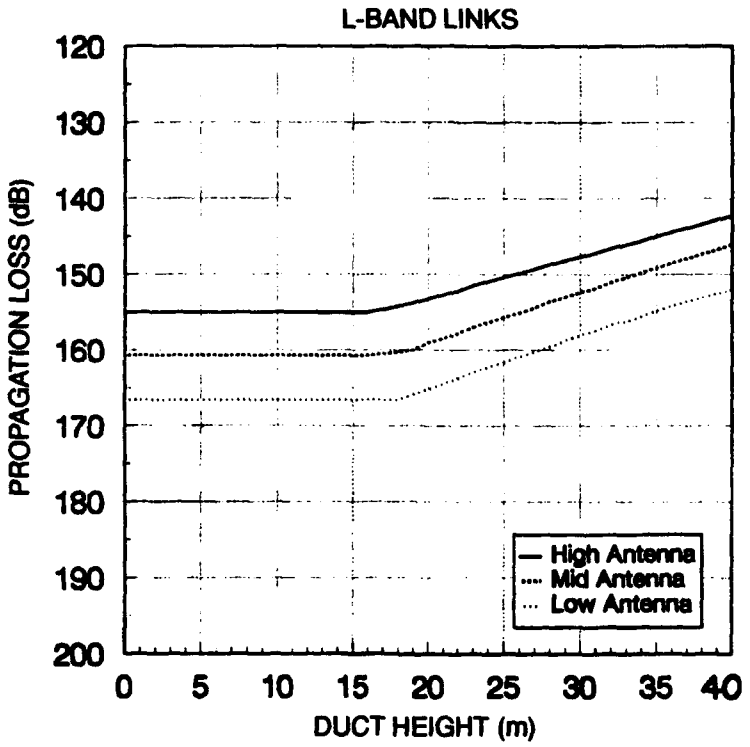

Figure 6. L-band propagation loss versus evaporation duct height.

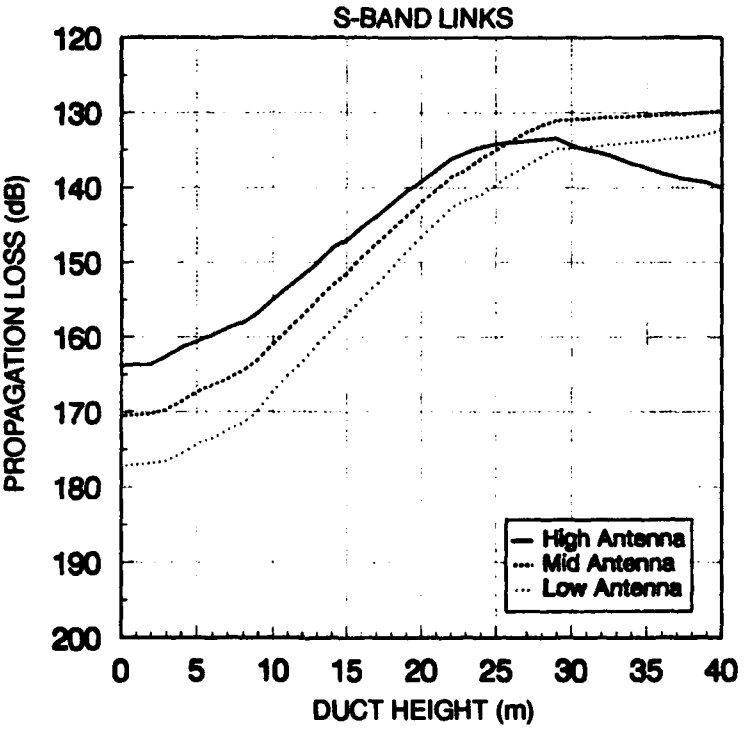

Figure 7. S-band propagation loss versus evaporation duct height.

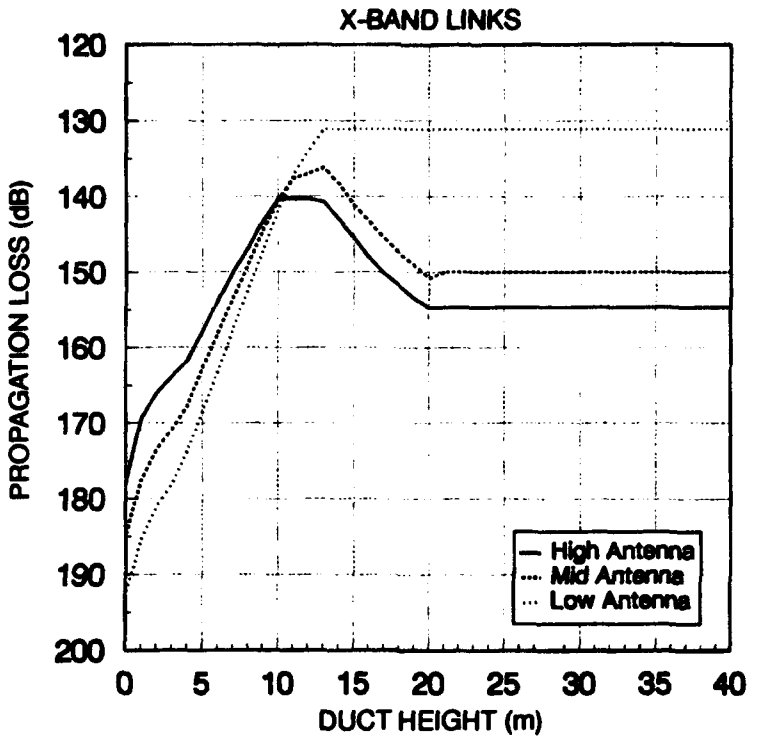

Figure 8. X-band propagation loss versus evaporation duct height.

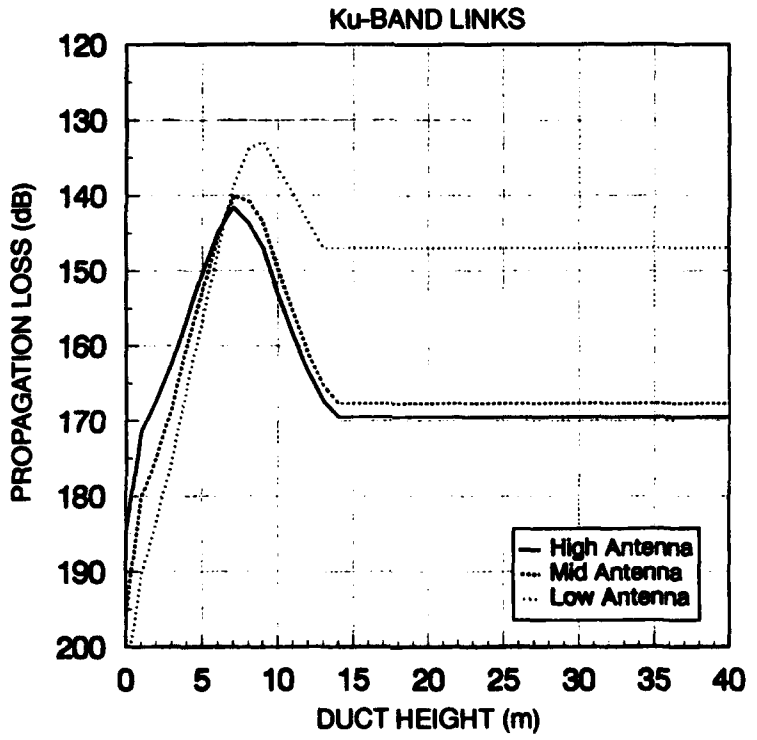

Figure 9. Ku-band propagation loss versus evaporation duct height.

EVAPORATION DUCT MODELS

For EREPS, two sets of evaporation duct heights were calculated: one according to the methods of *Jeske* (1973); the second according to the modification described by *Paulus* (1985). Figure 10 shows an overplot of duct height computed by both methods. The Jeske formulation yields the same duct heights as figure 1 of *Patterson* (1985). The modification to the Jeske duct heights changes the calculations only for certain stable, low-humidity conditions; that is, the spikes in Jeske duct height in figure 10 are correlated with the positive ASTD spikes (figure 5) that occur with lower relative humidities (figure 4). Such spikes often are observed as a distinct diurnal variation in operational data taken aboard ships (*Paulus*, 1989a). In the open ocean these spikes are spurious since such conditions exist only with the strong synoptic influences of offshore winds. Modified duct heights are shown in figure 11 for both Naxos and Mykonos. In general, duct heights for each location follow the same trends, although there are times of obvious differences.

As mentioned earlier, the EREPS evaporation duct propagation model is based on waveguide solutions using M profiles for neutral-stability conditions. Neutral conditions are a reasonable assumption in the open ocean, but figure 5 shows significant variations away from neutral (air temperature ≈ sea temperature). The question is whether, or not, it is valid to use EREPS under such conditions. Previous work has found that, for common departures from neutrality, the neutral profile is a reasonable approximation for full-wave calculations, provided that the duct height is determined from observed meteorology (*Anderson*, 1990). A sample of neutral M profiles calculated from a 6-hourly subset of the Mykonos meteorological data, along with a profile having a linear gradient of 0.13 M/m superimposed, is shown in figure 12. The latter is the M gradient for a well-mixed boundary layer. The general characteristics of these profiles are that the M deficit increases as duct height increases, and all profiles are to the left of the well-mixed profile. Also, duct heights are limited to 40 m and "negative duct heights," which correspond to subrefractive layers, are not permitted. (See Appendix A.)

Stability-dependent M profiles for RPO were calculated according to *Paulus* (1989b) with, and without, the modification to the Jeske formulation. A sample of profiles, calculated from the same 6-hourly Mykonos meteorological data as used for figure 12, is shown in figure 13. Some low ducts have large M deficits, and subrefractive profiles are possible, as evident by the profile to the right of the linear reference profile. Refractivity profiles were also calculated in accordance with *Liu and Blanc* (1984) and with a constant aerodynamic roughness parameter as in Anderson (1993).

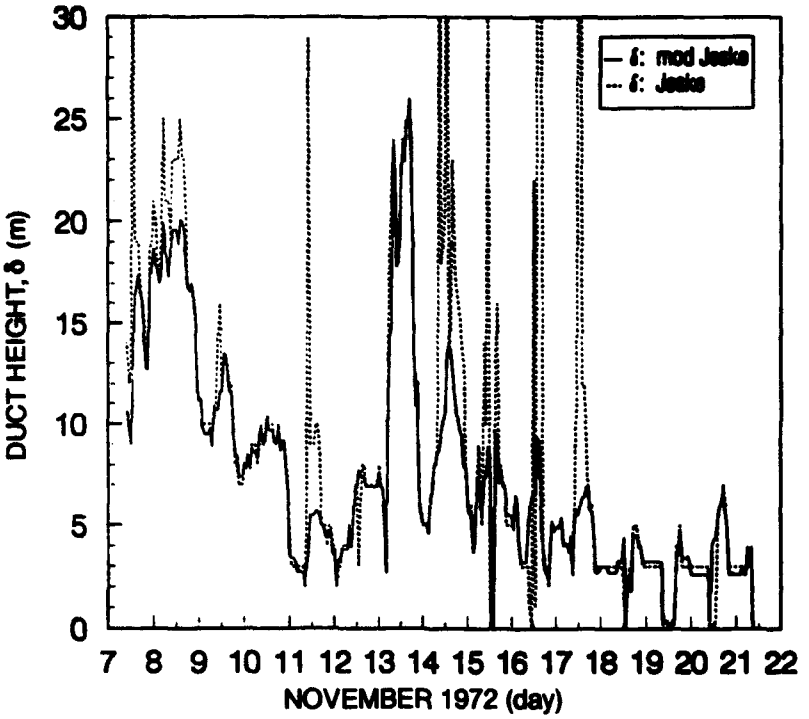

Figure 10. Evaporation duct height, δ, versus time at Mykonos, obtained by using the Jeske and the modified calculation.

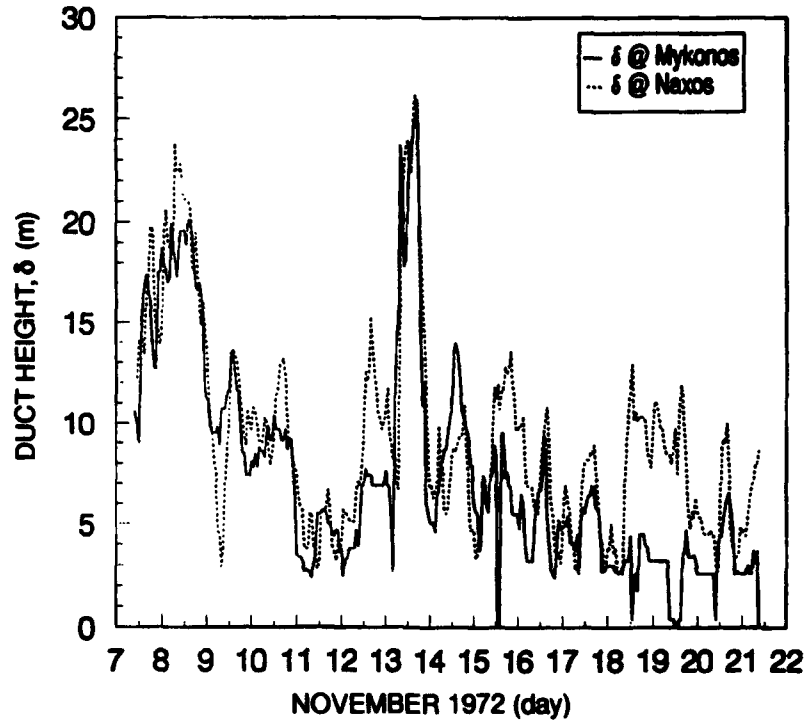

Figure 11. Evaporation duct height, δ, versus time at Mykonos and Naxos, obtained by using the modified calculation.

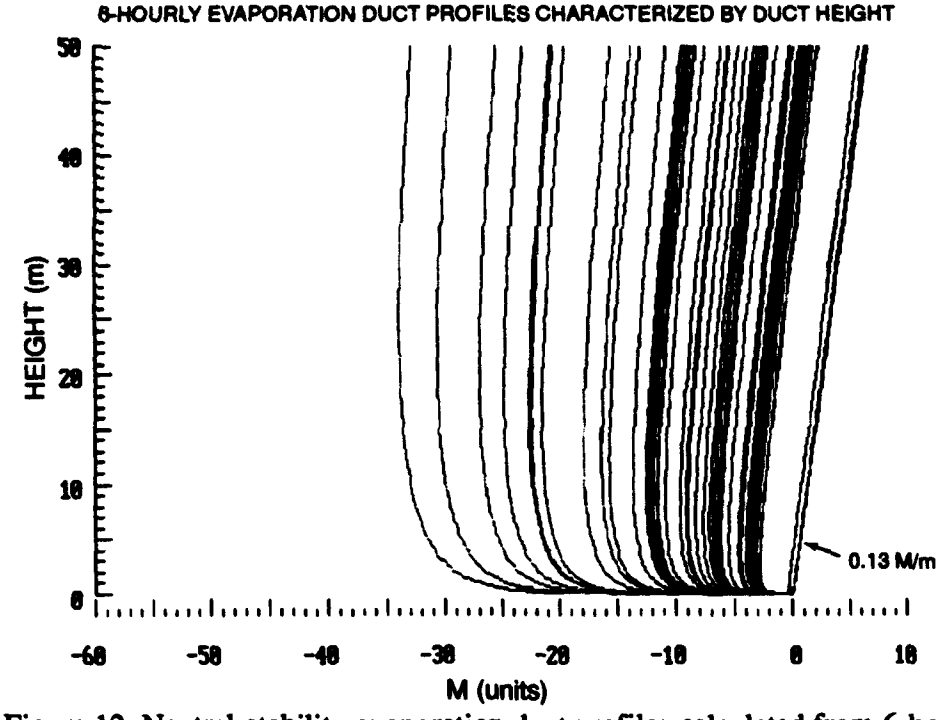

Figure 12. Neutral-stability evaporation duct profiles calculated from 6-hourly Mykonos evaporation duct height data. Profiles have been normalized to 0 at the surface. A linear gradient of 0.13 M/m is superimposed for comparison purposes.

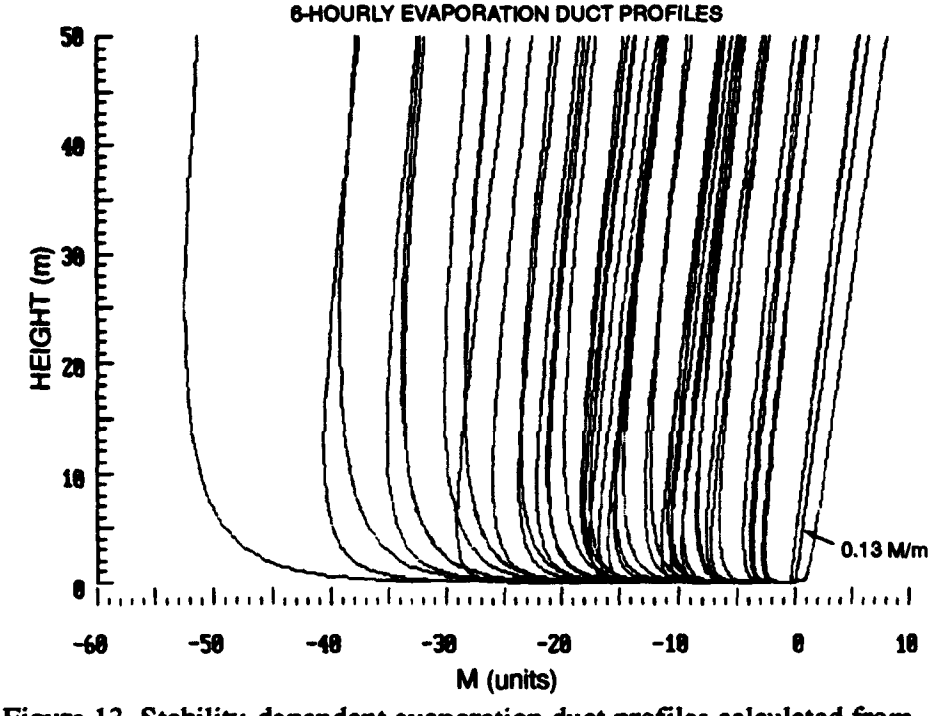

Figure 13. Stability-dependent evaporation duct profiles calculated from 6-hourly Mykonos meteorological data. Profiles have been normalized to 0 at the surface. A linear gradient of 0.13 M/m is superimposed for comparison purposes.

DATA ANALYSIS

OBJECTIVES

The objectives of the following data comparisons were to

(1) determine whether the modified evaporation duct calculation improved propagation loss predictions from point-observed data,

(2) determine whether RPO predictions with stability-dependent evaporation duct profiles were an improvement over the waveguide parameterization solutions using neutral-stability profiles (EREPS),

(3) determine whether characterization of range-varying evaporation duct conditions improved propagation loss predictions.

STATISTICAL COMPARISON TABLES

Numerous model runs were made with differing evaporation duct characterizations. Comparisons between observed and predicted propagation loss for the various combinations are summarized in tables 2, 3, and 4. The statistics shown in tables 2 and 4 are not precise because the calculations were done in decibels; however, the purpose of the statistics is comparison of models, and the calculations serve this purpose well.

The combinations, as shown in the column headings are as follows:

(1) EREPS Jeske—The EREPS model predictions with unmodified evaporation duct heights in meters (m) calculated from the Mykonos meteorological data, as represented by the dotted line in figure 10,

(2) EREPS mod δ—The EREPS model predictions with modified evaporation duct heights (using δ as shorthand for duct height) calculated from the Mykonos meteorological data, as represented by the solid line in figure 10,

(3) RPO RI Jeske—The RPO model run in the range-independent mode with stability-dependent profiles calculated from the Mykonos meteorological data following *Jeske* (1973),

(4) RPO RI mod δ—The RPO model run in the range-independent mode with stability-dependent profiles calculated from the Mykonos meteorological data following *Paulus* (1989b),

(5) RPO RI LKB—The RPO model run in the range-independent mode with stability-dependent profiles calculated from the Mykonos meteorological data using the surface-layer model of Liu, Katsaros, and Businger (*Liu and Blanc*, 1984) with a constant surface roughness parameter of 1.5 by 10^{-4} m,

(6) EREPS Naxos mod δ—The EREPS model predictions with modified evaporation duct heights calculated from the Naxos meteorological data, as represented by the dotted line in figure 11,

(7) RPO RD—The RPO model run in the range-dependent mode with stability-dependent profiles generated from both the Mykonos and Naxos meteorological data following *Paulus* (1989b).

Table 2. Linear correlation coefficients between predicted and observed propagation loss values.

LINEAR CORRELATION COEFFICIENTS								
Band	Ant. Ht.	(1) EREPS Jeske	(2) EREPS mod δ	(3) RPO RI Jeske	(4) RPO RI mod δ	(5) RPO RI LKB	(6) EREPS Naxos mod δ	(7) RPO RD
L	High	0.15	0.17	0.20	0.21	0.18	0.16	0.22
	Mid	0.17	0.18	0.22	0.25	0.19	0.20	0.25
	Low	0.21	0.22	0.28	0.29	0.21	0.25	0.27
S	High	0.42	0.45	0.39	0.45	0.39	0.46	0.48
	Mid	0.46	0.52	0.45	0.52	0.40	0.51	0.53
	Low	0.50	0.54	0.49	0.55	0.44	0.52	0.56
X	High	0.42	0.52	0.37	0.44	0.50	0.31	0.39
	Mid	0.55	0.66	0.60	0.70	0.66	0.43	0.68
	Low	0.69	0.77	0.68	0.77	0.72	0.59	0.76
Ku	High	0.21	0.34	0.14	0.10	0.17	0.12	0.11
	Mid	0.31	0.37	0.28	0.29	0.31	–0.03	0.32
	Low	0.49	0.60	0.49	0.57	0.54	0.23	0.59

Table 3. Percent of time that the absolute difference between predicted and observed propagation loss is 10 dB or less.

PERCENT OF TIME |OBS – PRED| ≤ 10 dB								
Band	Ant. Ht.	(1) EREPS Jeske	(2) EREPS mod δ	(3) RPO RI Jeske	(4) RPO RI mod δ	(5) RPO RI LKB	(6) EREPS Naxos mod δ	(7) RPO RD
L	High	97	97	79	87	93	97	83
	Mid	97	99	84	94	94	99	92
	Low	98	99	81	91	95	99	88
S	High	75	81	77	85	89	90	85
	Mid	73	81	71	79	89	84	81
	Low	60	68	71	78	78	77	83
X	High	58	66	65	71	65	72	74
	Mid	55	61	66	71	56	55	74
	Low	56	64	58	64	52	50	67
Ku	High	60	72	69	73	66	65	77
	Mid	52	63	58	64	59	51	69
	Low	59	60	51	58	54	53	65

Table 4. Root-mean-square differences (dB) between predicted and observed propagation loss.

RMS DIFFERENCE BETWEEN PREDICTED AND OBSERVED PL								
Band	Ant. Ht.	(1) EREPS Jeske	(2) EREPS mod δ	(3) RPO RI Jeske	(4) RPO RI mod δ	(5) RPO RI LKB	(6) EREPS Naxos mod δ	(7) RPO RD
L	High	5.2	4.8	9.2	6.9	8.8	4.9	7.3
	Mid	4.6	4.1	8.6	6.0	8.7	4.2	6.3
	Low	5.0	4.5	8.8	6.2	9.0	4.6	6.6
S	High	9.1	8.3	9.6	7.8	8.7	7.5	7.3
	Mid	10.4	8.8	11.0	8.4	9.6	8.1	8.0
	Low	11.6	10.4	12.1	9.1	11.2	9.4	8.3
X	High	11.6	10.5	13.0	11.2	13.0	9.6	8.9
	Mid	13.2	11.7	13.5	11.0	14.6	12.1	9.1
	Low	14.3	12.1	14.9	11.9	15.4	14.5	10.6
Ku	High	12.8	10.5	14.8	12.1	15.9	10.4	8.5
	Mid	15.2	12.9	17.4	14.3	18.8	12.5	9.5
	Low	17.0	14.4	20.2	16.4	21.5	15.7	11.7

All correlation coefficients in table 2 for L-, S-, and X-bands are significant at the 99 percent confidence level. All correlation coefficients for Ku-band are also significant at the 99 percent confidence level, except for the following: (3) RPO RI Jeske, (6) EREPS Naxos mod δ, and (7) RPO RD for the High antenna (all three significant for the 95 percent confidence level); (4) RPO RI mod δ for the High antenna and (6) EREPS Naxos mod δ for the Mid antenna (not significant at 95 percent confidence level).

A correlation coefficient by itself is not necessarily indicative of how good of a propagation prediction it is. Table 3 shows the percent of time that the predicted propagation loss was within 10 dB of the observed propagation loss, and table 4 shows the root-mean-square difference between predicted and observed propagation loss. Most notably, L-band correlations were the weakest, but predicted propagation loss is within 10 dB of observed more than 80 percent of the time and the rms differences are the smallest. This is not unexpected, because L-band signal variations are not strongly influenced by evaporation ducting and the dynamic range of the L-band signal during the 2-week period was 26 dB (table 5). Conversely, the X-band, low antenna predictions, which have the highest correlations with the observations, are within 10 dB a lesser percentage of the time and rms differences are larger; however, the dynamic range of the X-band signal was nearly 77 dB. The statistics in tables 3 and 4 should be considered with respect to the dynamic range of the observed propagation loss on each link; for example, someone interpreting these statistics must qualitatively judge whether or not predictions that are within 10 dB of observed for 91 percent of the time (for an L-band signal that varies over a dynamic range of 24.5 dB) are as good as predictions that are within 10 dB of observed for 64 percent of the time (for an X-band signal that varies over a dynamic range of 76.8 dB).

Table 5. Observed dynamic range (dB) and number of observations for each link.

PROPAGATION LOSS OBSERVATIONS (Obs)			
Band	Ant. Ht.	Dynamic Range (dB)	No. Obs.
L	High	24.2	306
	Mid	26.1	305
	Low	24.8	306
S	High	37.0	272
	Mid	40.8	271
	Low	44.9	274
X	High	40.4	314
	Mid	63.9	314
	Low	76.8	314
Ku	High	36.6	233
	Mid	45.9	231
	Low	54.5	231

SIGNIFICANCE OF THE MODIFIED EVAPORATION DUCT CALCULATION

Statistical assessment capabilities of the EREPS propagation model and annual distributions of modified evaporation duct height were demonstrated by *Hitney and Vieth* (1990) and *Hitney and Hitney* (1990). Here, the first objective, to determine whether the modified evaporation duct calculation improved propagation loss predictions from point-observed data, was approached by comparing EREPS predictions (using the Jeske duct height) with predictions (using the modified duct height) against measured radio data. Similarly, RPO predictions using Jeske profiles can be compared with predictions using a modified calculation of the profiles. Examples of each, for S-band, are shown in figures 14 and 15 along with the free space level at 132.9 dB and standard diffraction level at 178 dB. The most obvious difference in figure 14 is that the unmodified calculations yield anomalously low propagation loss values (approaching and exceeding free space levels) corresponding to the spikes in the Jeske duct heights in figure 10. Similar features are apparent in figure 15, but now the unmodified calculations result in more anomalously high propagation loss values (exceeding diffraction) than the modified calculations indicate. Smaller differences in predictions also occur, but both model predictions generally follow the longer-time-scale trends in the data.

Comparing the correlation coefficients for the EREPS predictions using the Jeske duct height, table 2, column (1) EREPS Jeske, with the correlation coefficients for the EREPS predictions using the modified duct height of table 2, column (2) EREPS mod δ, shows that the latter are consistently greater than those for EREPS Jeske. Tests of significance show these differences for X-band to be significant at the 90 percent, or greater, confidence level in table 6, column (1). Similarly, comparing the correlation coefficients for the RPO range-independent predictions using Jeske profiles of table 2, column (3) RPO RI Jeske, with the correlation coefficients for the RPO range-independent predictions using a modified calculation of the profiles in table 2, column (4) RPO RI mod δ, demonstrates the latter are consistently greater than those for RPO RI Jeske and are significant at the levels indicated in table 6, column (2).

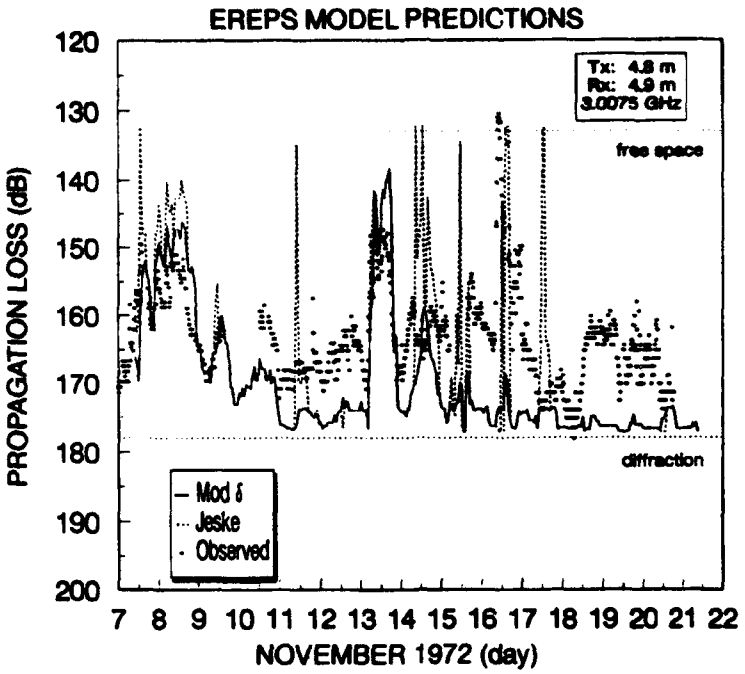

Figure 14. Predicted propagation loss versus time, by using the EREPS model with and without the modified evaporation duct height calculation, plotted with observed propagation loss for the low, S-band, receiving antenna.

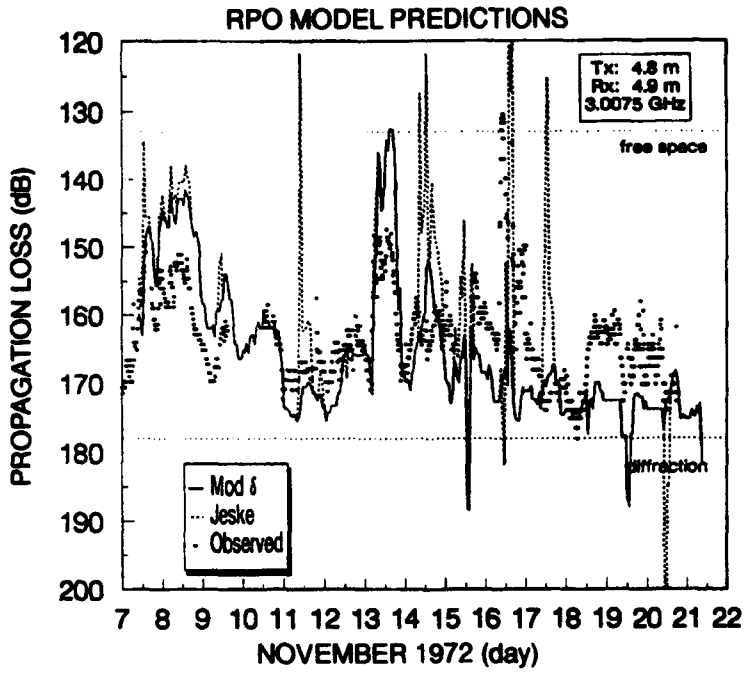

Figure 15. Predicted propagation loss versus time, by using the RPO model with and without the modified evaporation duct height calculation, plotted with observed propagation loss for the low, S-band, receiving antenna.

Table 6. Confidence levels for significant differences between correlation coefficients. NS indicates not significant at 68 percent confidence level or higher.

CONFIDENCE LEVEL (%) OF CORRELATION COEFFICIENT DIFFERENCES			
Band	Ant. Ht.	(1) EREPS mod δ: EREPS Jeske	(2) RPO RI mod δ: RPO RI Jeske
L	High	NS	NS
	Mid	NS	NS
	Low	NS	NS
S	High	NS	NS
	Mid	NS	68
	Low	NS	68
X	High	90	68
	Mid	95	95
	Low	95	95
Ku	High	80	NS
	Mid	NS	NS
	Low	90	68

Comparing the percent of time that the EREPS predictions using the modified duct height of table 3, column (2) EREPS mod δ, are within 10 dB of observed with the percent of time for EREPS using the unmodified duct height in table 3, column (1) EREPS Jeske, shows the accuracy using the modified duct height to be consistently higher than when using the unmodified duct height. Table 4 shows EREPS using the modified duct height, column (2), yields smaller rms differences than using the unmodified duct height, column (1). Similarly, the range-independent RPO percentages are higher in table 3, columns (3) and (4), and rms differences less in table 4, columns (3) and (4), using the modified profiles than when using the unmodified profiles.

The conclusion is that the modified evaporation duct calculation, originally developed using data from an independent Ku-band propagation link, has skill in improving point-by-point propagation predictions at all frequencies.

SIGNIFICANCE OF STABILITY-DEPENDENT PROFILES

An assumption in the EREPS propagation models is that the "evaporation duct height" is the dominant factor in characterizing the evaporation duct, thereby allowing parameterization of evaporation duct propagation based on waveguide solutions at 9.6 GHz (*Patterson et al.*, 1990). Thermal stability of the surface layer is thus assumed to be a secondary influence. The second objective was to determine whether or not RPO predictions with stability-dependent evaporation duct profiles were an improvement over the waveguide parameterization solutions using neutral-stability profiles (EREPS). This can be tested partly by comparing the statistics for EREPS using the modified duct height (2) EREPS mod δ with the statistics for RPO in the

range-independent mode using stability-dependent profiles calculated with the modified duct algorithm (4) RPO RI mod δ. The correlation coefficients in table 2, column (2) versus column (4), show no consistent trend between these two categories: the RPO correlations are mixed at X-band; and EREPS correlations are greater at Ku-band; however, for the most part, the differences between the correlation coefficients for these two categories are not significant as shown by column (1) in table 7. Similarly, comparison of tables 3 and 4, column (2) versus column (4), show no consistent trend in the accuracy of one model over the other.

Table 7. Confidence levels for significant differences between correlation coefficients. NS indicates not significant at the 68 percent confidence level or higher.

CONFIDENCE LEVEL (%) OF CORRELATION COEFFICIENT DIFFERENCES				
Band	Ant. Ht.	(1) EREPS mod δ: RPO RI mod δ	(2) RPO RI mod δ: RPO RI LKB	(3) RPO RI Jeske: RPO RI LKB
L	High	NS	NS	NS
	Mid	NS	NS	NS
	Low	NS	NS	NS
S	High	NS	NS	NS
	Mid	NS	90	NS
	Low	NS	90	NS
X	High	80	68	95
	Mid	NS	NS	68
	Low	NS	80	NS
Ku	High	99	NS	NS
	Mid	NS	NS	NS
	Low	NS	NS	NS

This comparison is complicated by the EREPS single mode assumption; differences in predictions could be due to either stability effects on the profile or multimode propagation for which EREPS does not account. So, further comparisons can be made between RPO in the range-independent mode using stability-dependent profiles calculated from the modified duct algorithm (4) RPO RI mod δ, and the LKB surface-layer model (5) RPO RI LKB. The LKB model is a more physically rigorous surface-layer model than that used by Jeske. Table 2 shows the correlation coefficients for the RPO calculations using the modified profile algorithm RPO RI mod δ to be greater than those for LKB model (5) RPO RI LKB in 9 of 12 cases, column (4) versus column (5); however, table 7, column (2), shows these differences to be significant in only four cases, and (5) RPO RI LKB to be superior for the high, X-band. Table 3 shows (4) RPO RI mod δ with the modified profiles to be within 10 dB of the observed data more often (6 of 12 cases, 2 ties) than with unmodified profiles (5) RPO RI LKB, column (4) versus column (5), and table 4 shows RPO with modified profiles yield consistently smaller rms differences, column (4) versus column (5).

A more appropriate comparison would be to match RPO predictions using profiles generated by using Jeske's approach with RPO predictions using the more physically rigorous LKB model,

because neither one does any modifications to the evaporation duct calculations. Table 2 shows correlation coefficients of (3) RPO RI Jeske to be larger than those of (5) RPO RI LKB for L- and S-bands; the opposite is true for X- and Ku-bands, column (3) versus column (5); however, the differences are significant only for the High, and Mid, X-band antennas as shown in table 7, column (3). Table 3 shows (5) RPO RI LKB to be within 10 dB of the observed data more often, 7 of 12 cases for column (3) versus column (5), but table 4 shows (3) RPO RI Jeske to have smaller rms differences (7 of 12 cases) for column (3) versus column (5). Thus far, statistics show no significant stability-dependent effects.

To pursue this further, predicted propagation losses for (2) EREPS mod δ and (4) RPO RI mod δ (referred to in figures 16 to 27 as EREPS and RPO RI) and RPO RD (to be discussed in the next section) are plotted with observed propagation loss versus time. The free-space and diffraction levels, dotted and dashed lines, respectively, for each of the links is overplotted for reference. A qualitative impression is that above L-band, both the EREPS and RPO RI predictions follow the longer-time scale variations in the data equally well. For the most part, at L-band, EREPS predicts standard diffraction level; RPO in the range-independent mode does exhibit variations in propagation loss.

Another perspective of the data is obtained by plotting ogives, figures 27 through 39, of the predicted and observed data shown in figures 16 to 27, respectively. The ogives were calculated from histograms of propagation loss in one-decibel bins. For L-band, RPO RI propagation loss predictions are consistently less than EREPS that are consistently less than the observed. (The observed distribution is low compared to diffraction; this discrepancy could be due to either boundary layer gradients that the surface layer models of refractivity do not account for or unaccounted losses in the L-band hardware.) The S-band ogives are all consistent in showing that even though EREPS is a very good predictor compared to diffraction, RPO range-independent calculations are a better match to the observed distribution. The X-band ogives show EREPS and RPO RI to be comparable. At Ku-band, EREPS and RPO RI are comparable, except around median levels for the Mid antenna. This difference may be due to multimode propagation. Both models consistently underestimate propagation losses at lower propagation loss values (stronger evaporation ducting) with the greatest discrepancies occurring for the Low antenna. This may be indicative of the lack of a surface roughness model for the over-the-horizon regions in EREPS and RPO (version 1.14).

The conclusion is that stability-dependent evaporation duct profiles do not make a significant difference in propagation loss predictions for this data set. This is due to several considerations, including

(1) The path may have been essentially "open-ocean," and stability variations may not have been strong or frequent enough to be significant, even though the propagation path is between two islands in the Aegean Sea and the large land masses of Greece and Turkey are only a little over 100 km away

(2) We should not expect the coarse meteorological measurements for this experiment to accurately estimate stability. *Blanc* (1987) concluded that bulk determination of stability yields only a very crude estimate of the true stability influence. The bulk meteorological measurements on Mykonos and Naxos were not made in the best locations or with consistent temporal resolution. Also, linear interpolation to hourly observations may have masked stability influences.

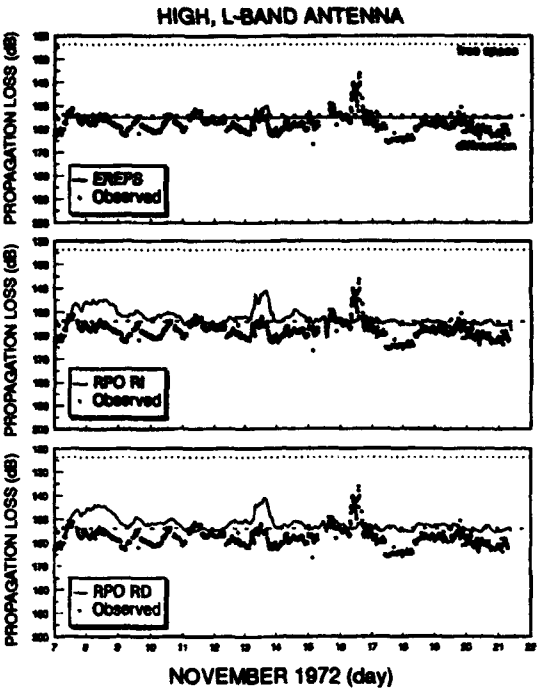

Figure 16. Comparison of observed and predicted propagation loss for the high, L-band antenna. Upper frame—EREPS predictions, middle frame—RPO range-independent predictions, and lower frame—RPO range-dependent predictions.

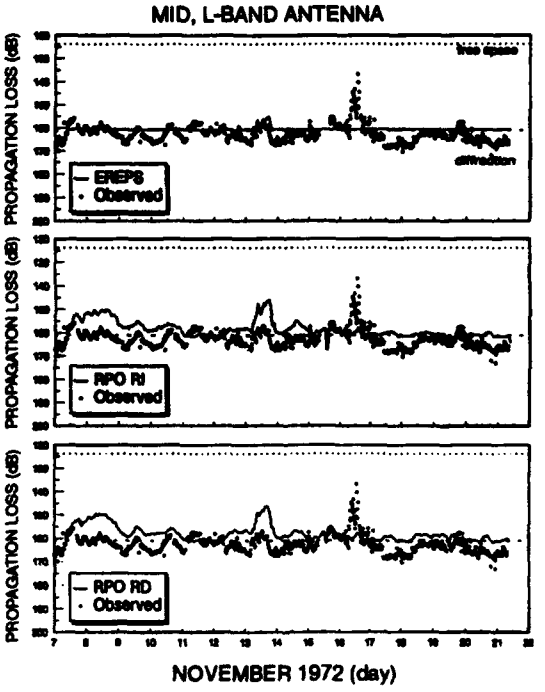

Figure 17. Comparison of observed and predicted propagation loss for the mid, L-band antenna. Upper frame—EREPS predictions, middle frame—RPO range-independent predictions, and lower frame—RPO range-dependent predictions.

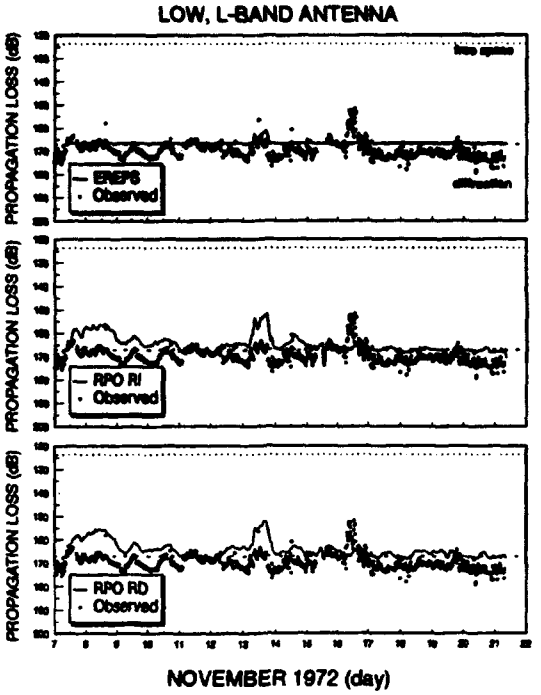

Figure 18. Comparison of observed and predicted propagation loss for the low, L-band antenna. Upper frame—EREPS predictions, middle frame—RPO range-independent predictions, and lower frame—RPO range-dependent predictions.

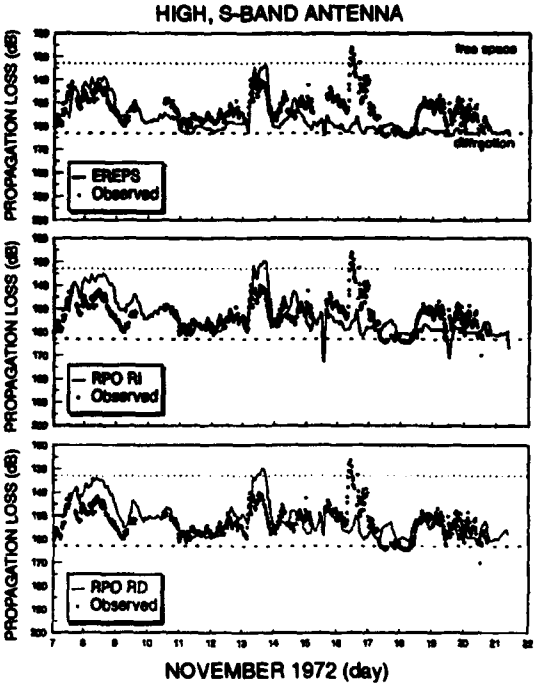

Figure 19. Comparison of observed and predicted propagation loss for the high, S-band antenna. Upper frame—EREPS predictions, middle frame—RPO range-independent predictions, and lower frame—RPO range-dependent predictions.

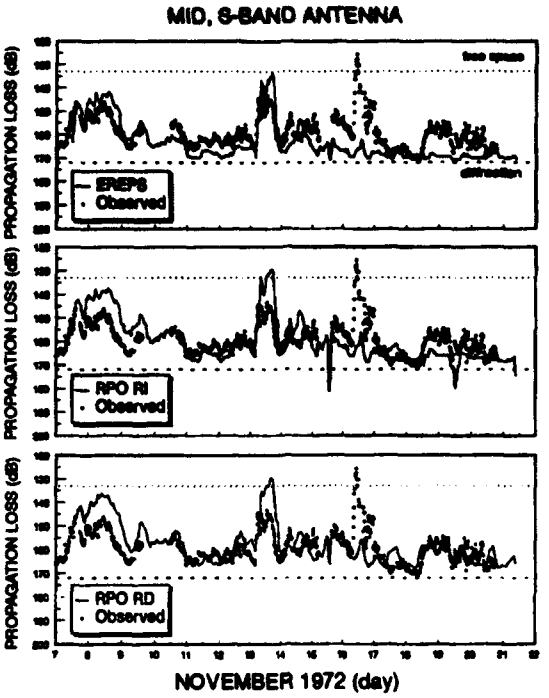

Figure 20. Comparison of observed and predicted propagation loss for the mid, S-band antenna. Upper frame—EREPS predictions, middle frame—RPO range-independent predictions, and lower frame—RPO range-dependent predictions.

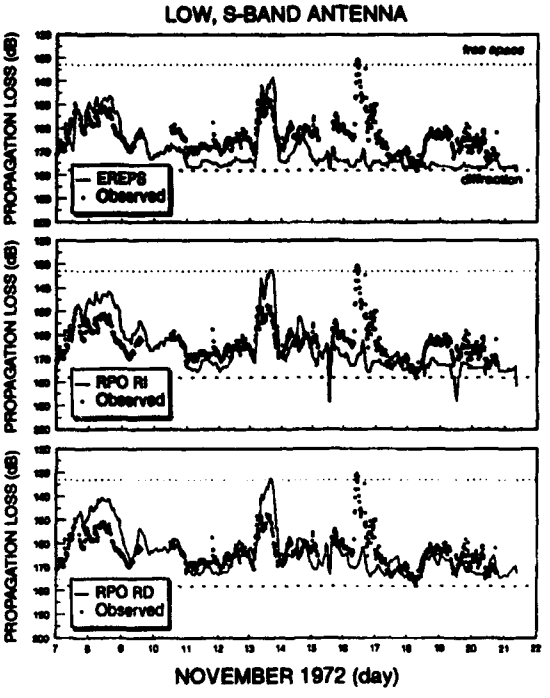

Figure 21. Comparison of observed and predicted propagation loss for the low, S-band antenna. Upper frame—EREPS predictions, middle frame—RPO range-independent predictions, and lower frame—RPO range-dependent predictions.

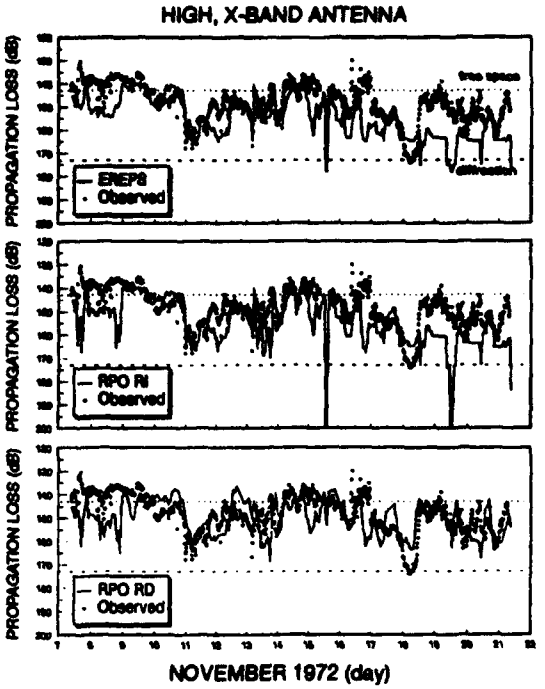

Figure 22. Comparison of observed and predicted propagation loss for the high, X-band antenna. Upper frame—EREPS predictions, middle frame—RPO range-independent predictions, and lower frame—RPO range-dependent predictions.

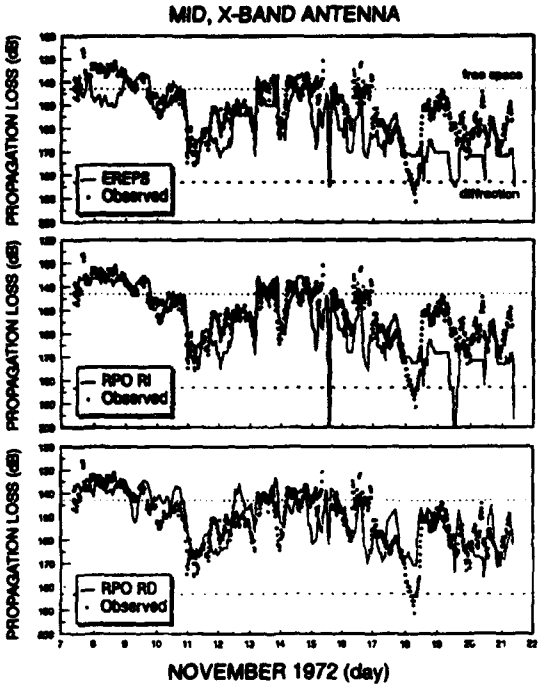

Figure 23. Comparison of observed and predicted propagation loss for the mid, X-band antenna. Upper frame—EREPS predictions, middle frame—RPO range-independent predictions, and lower frame—RPO range-dependent predictions.

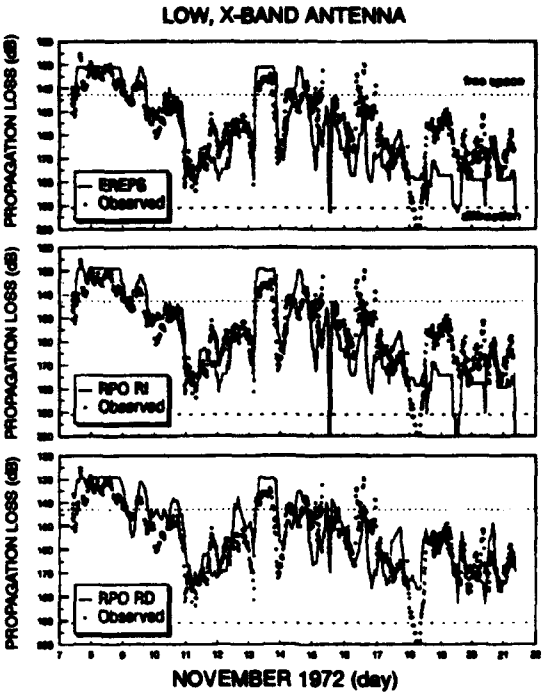

Figure 24. Comparison of observed and predicted propagation loss for the low, X-band antenna. Upper frame—EREPS predictions, middle frame—RPO range-independent predictions, and lower frame—RPO range-dependent predictions.

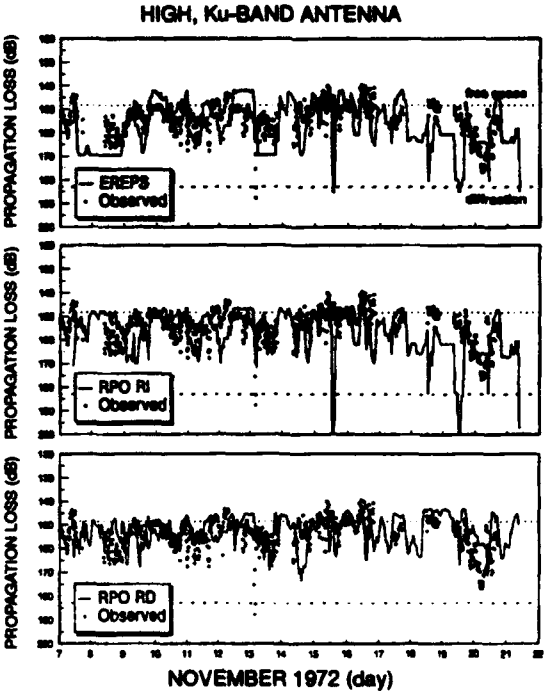

Figure 25. Comparison of observed and predicted propagation loss for the high, Ku-band antenna. Upper frame—EREPS predictions, middle frame—RPO range-independent predictions, and lower frame—RPO range-dependent predictions.

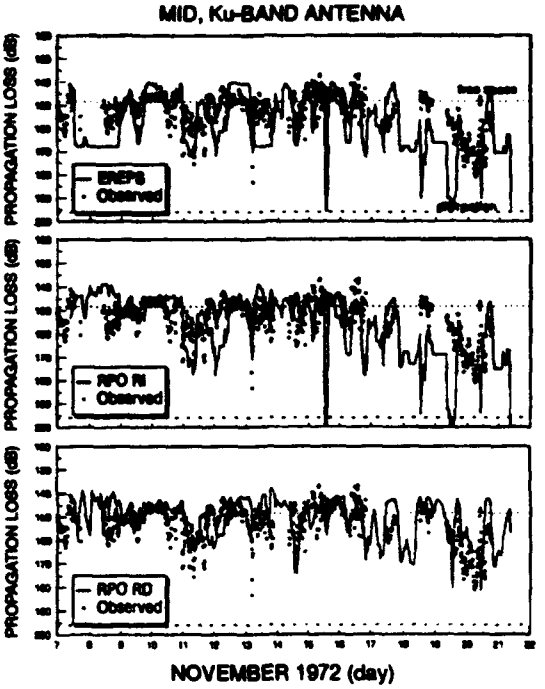

Figure 26. Comparison of observed and predicted propagation loss for the mid, Ku-band antenna. Upper frame—EREPS predictions, middle frame—RPO range-independent predictions, and lower frame—RPO range-dependent predictions.

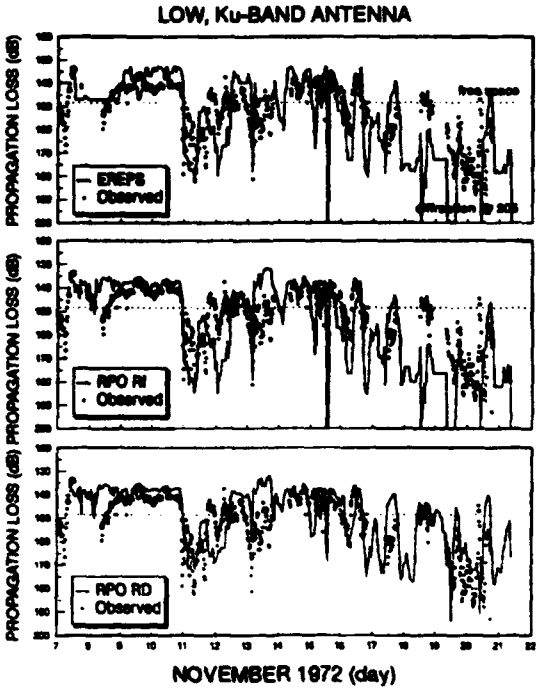

Figure 27. Comparison of observed and predicted propagation loss for the low, Ku-band antenna. Upper frame—EREPS predictions, middle frame—RPO range-independent predictions, and lower frame—RPO range-dependent predictions.

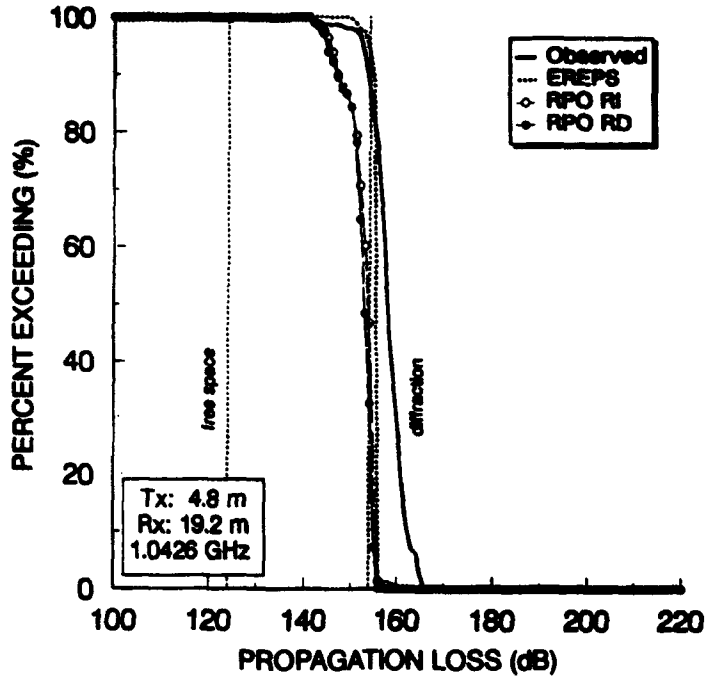

Figure 28. Cumulative frequency distributions of observed and predicted propagation loss for the high, L-band antenna.

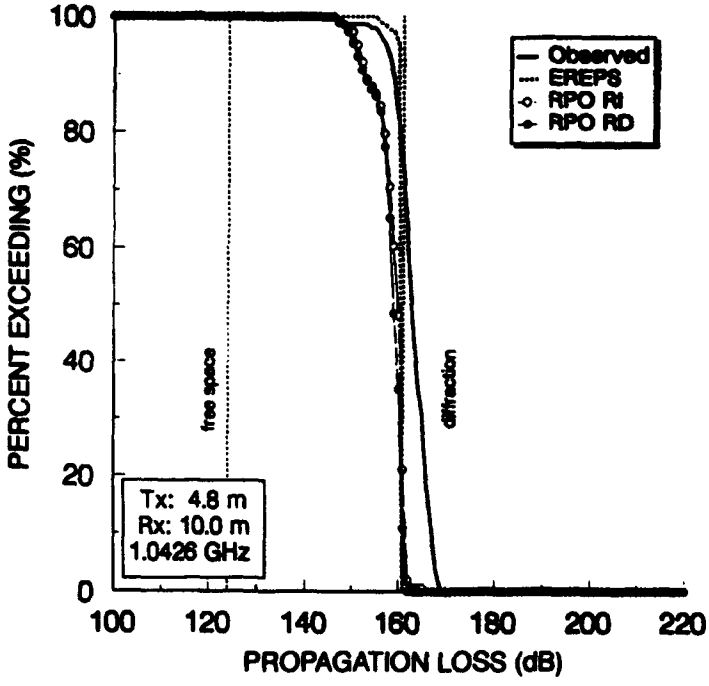

Figure 29. Cumulative frequency distributions of observed and predicted propagation loss for the mid, L-band antenna.

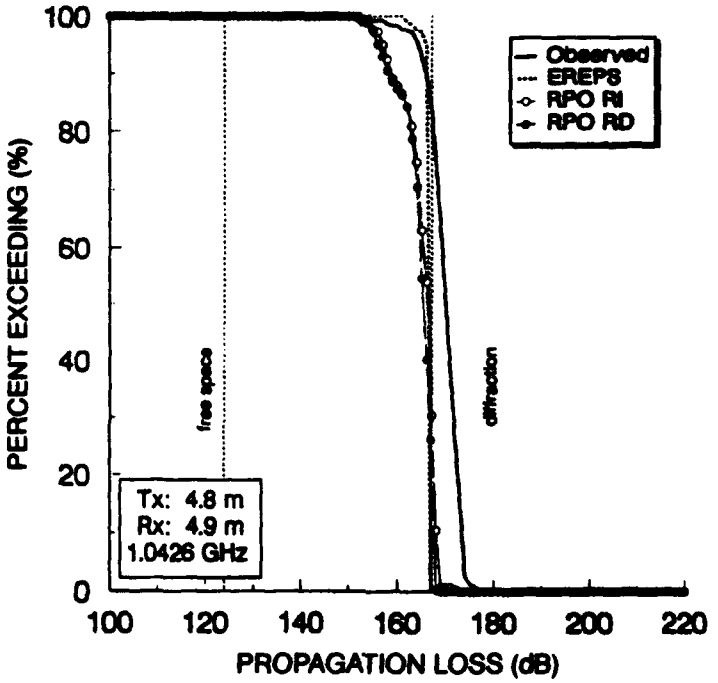

Figure 30. Cumulative frequency distributions of observed and predicted propagation loss for the low, L-band antenna.

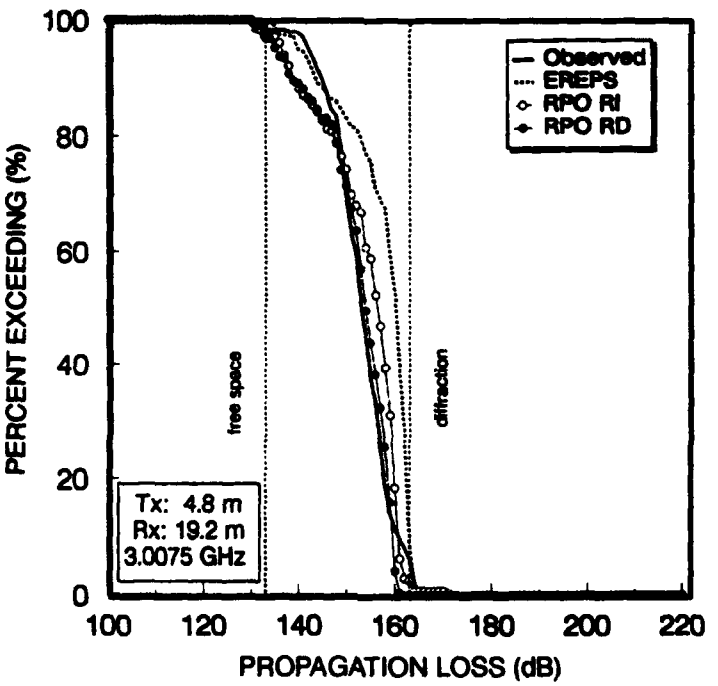

Figure 31. Cumulative frequency distributions of observed and predicted propagation loss for the high, S-band antenna.

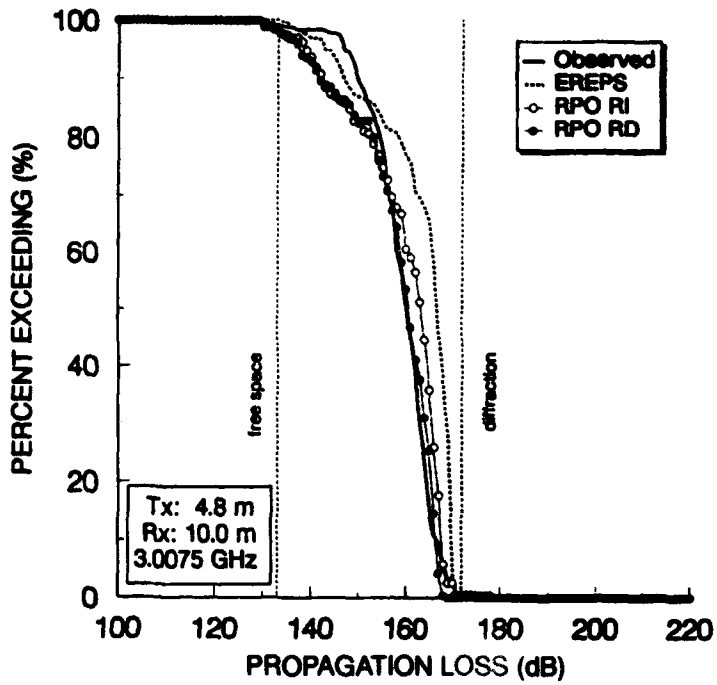

Figure 32. Cumulative frequency distributions of observed and predicted propagation loss for the mid, S-band antenna.

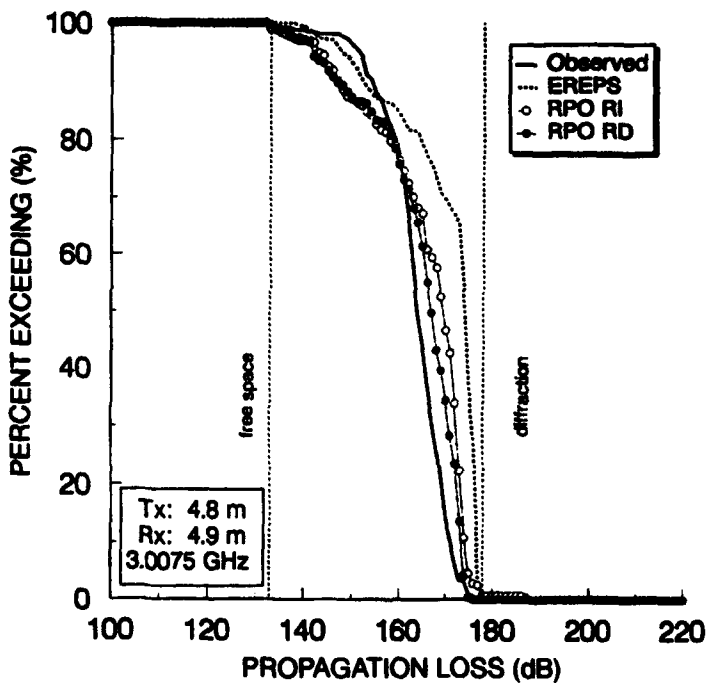

Figure 33. Cumulative frequency distributions of observed and predicted propagation loss for the low, S-band antenna.

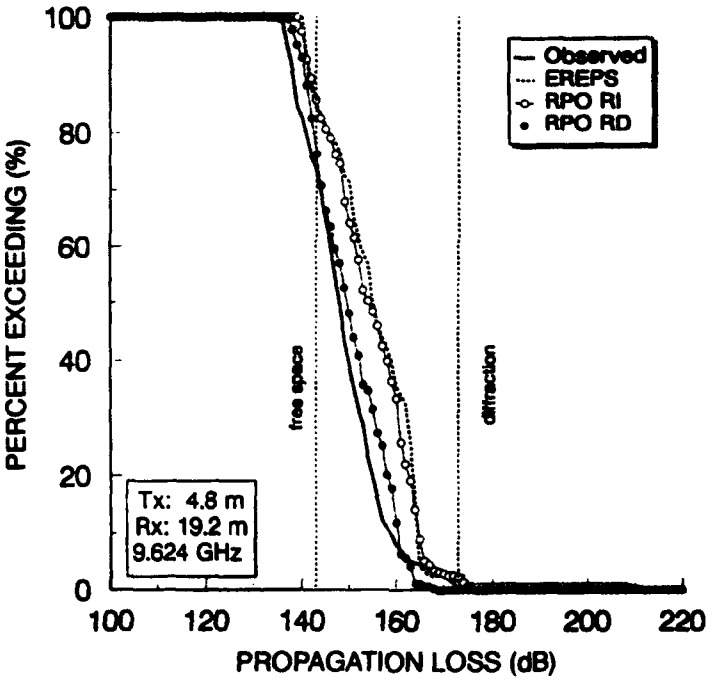

Figure 34. Cumulative frequency distributions of observed and predicted propagation loss for the high, X-band antenna.

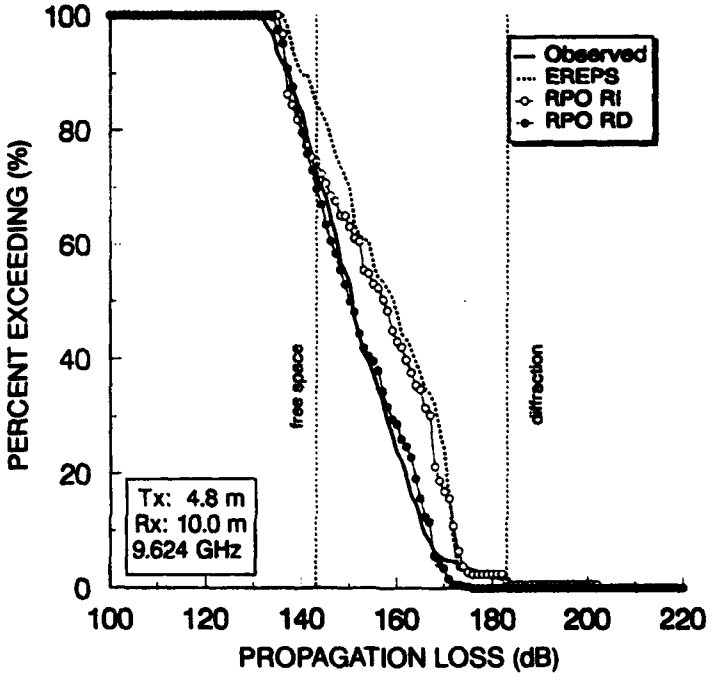

Figure 35. Cumulative frequency distributions of observed and predicted propagation loss for the mid, X-band antenna.

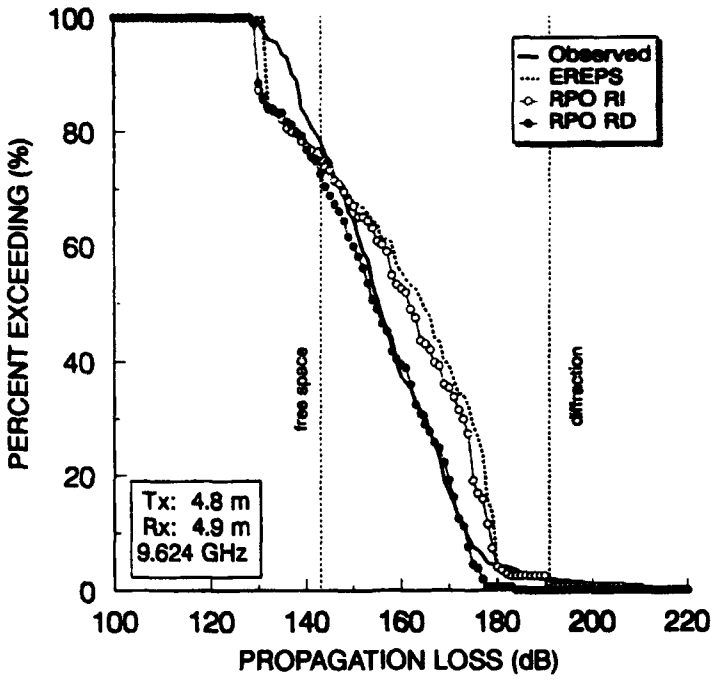

Figure 36. Cumulative frequency distributions of observed and predicted propagation loss for the low, X-band antenna.

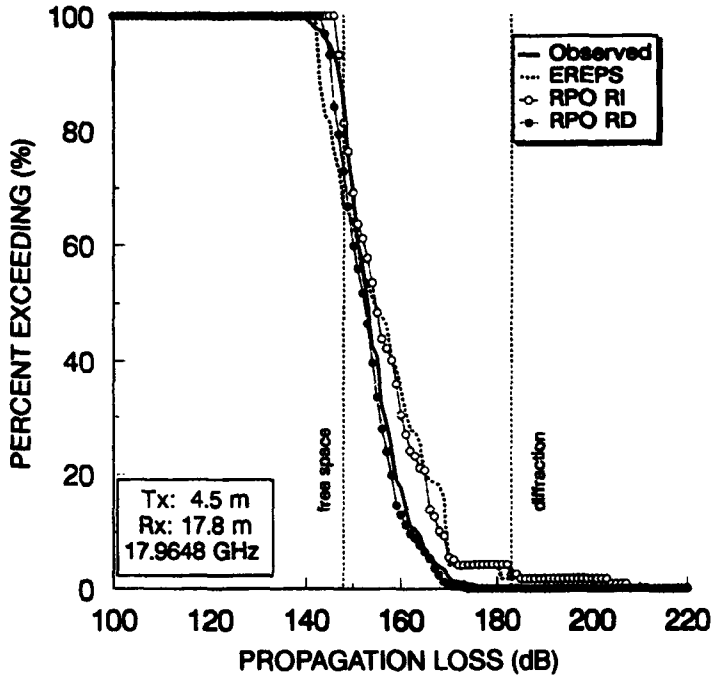

Figure 37. Cumulative frequency distributions of observed and predicted propagation loss for the high, Ku-band antenna.

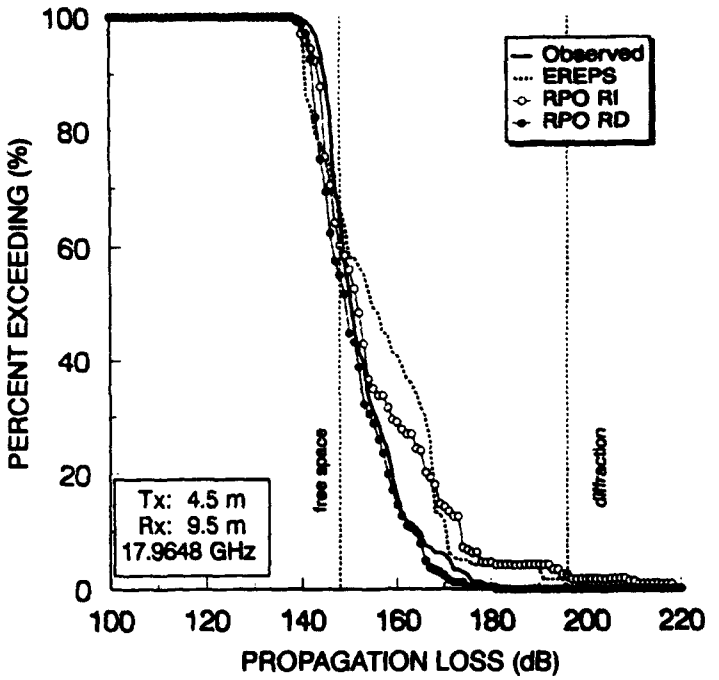

Figure 38. Cumulative frequency distributions of observed and predicted propagation loss for the mid, Ku-band antenna.

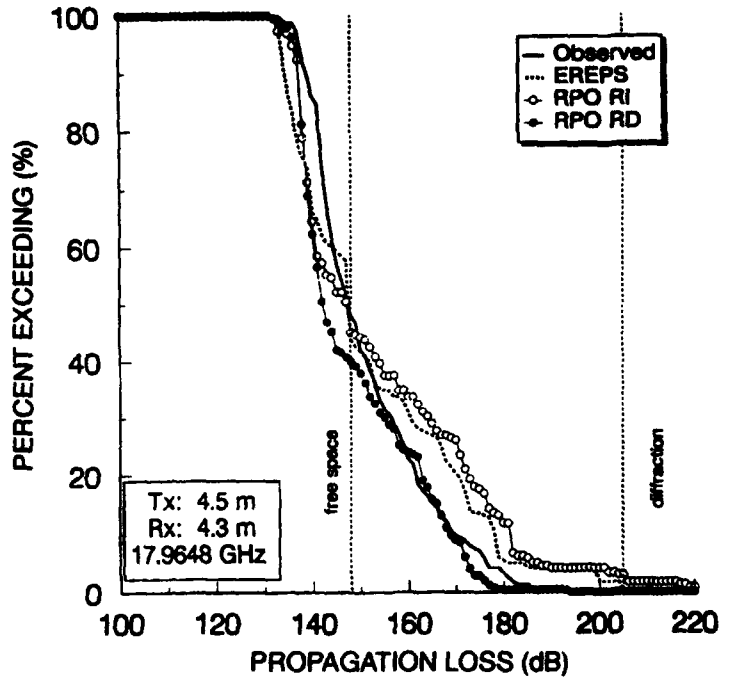

Figure 39. Cumulative frequency distributions of observed and predicted propagation loss for the low, Ku-band antenna.

SIGNIFICANCE OF RANGE-VARYING REFRACTIVE PROFILES

The availability of meteorological data on both Naxos and Mykonos made it possible to run RPO in the range-dependent mode. Figures 1 through 5 and figure 11 show differences in the measured conditions on the two islands. A representative estimate of the Naxos data for the propagation path can be made by comparing the EREPS run with the Mykonos data ([2] EREPS mod δ) with EREPS run with the Naxos data, (6) EREPS Naxos mod δ. The differences in correlation coefficients in table 2, column (2) versus column (6), are not significant for L- and S-bands; however, the differences are significant at the 99 percent confidence level for X- and Ku-bands. A similar trend is seen in table 3, column (2) versus column (6); no clear trend is seen in table 4, column (2) versus column (6). The implication of these comparisons is that the Mykonos meteorological data are more representative of the propagation path than Naxos data. This is not surprising considering that the Naxos weather station is not on the coast and the data is compiled from 3-hourly wind measurements and twice daily water temperature measurements. What is surprising is that the predictions based on the Naxos data are as good as they are.

For the range-dependent RPO runs (7) RPO RD, the Naxos profile was used at range zero and the Mykonos profile was used at range 35.2 km. RPO (version 1.14) uses the wind speed at range zero to model surface roughness effects for the ray-optics submodels (the PE submodel in RPO does not explicitly account for surface roughness). The RPO range-independent runs used the Mykonos wind speed. This differing characterization of surface roughness is not expected to have significant effect on the propagation loss predictions, except possibly at the Ku-band. The EREPS propagation models are analogous to RPO with respect to implementation of rough surface effects; for example, rough surface effects are accommodated in the optical region, but the parameterized wave-guide calculations for the diffraction region do not consider rough ocean surfaces.

Comparing the correlation coefficients for RPO RI mod δ and RPO RD in table 2, column (4) versus column (7), shows no trends and the differences between correlation coefficients are not significant. Table 3, column (4) versus column (7), shows that, except for L-band, RPO RD is consistently within 10 dB of observed propagation loss more frequently than RPO RI mod δ; table 4, column (4) versus column (7), yields a similar result. Figures 16 to 27 show RPO RD had little impact at L-band, but very noticeably improved the predictions in the other bands for the time period from mid-day on 18 November to 21 November. This is consistent with the greatest differences in duct heights in figure 11. In figures 28 to 39, the ogives for the RPO range-dependent calculations are clearly superior.

The conclusion is that the effects of range-varying evaporation duct structure were present and could be represented even with the shortcomings in the meteorological data available.

CONCLUSIONS

The objectives of this analysis were to investigate the effects of (1) a modified evaporation duct calculation, (2) surface-layer stability on propagation predictions, and (3) range-varying evaporation duct structure.

The modification to the Jeske surface-layer calculations was shown to improve point-by-point predictions of propagation loss in an ocean environment that is probably best classified as open ocean. This modification, based on the assumption that relatively warm, dry air does not occur in the open ocean surface layer, may fail in coastal regions where such conditions will exist when driven by synoptic patterns. Concurrent and consistent surface and upper air meteorological measurements will be required to characterize these conditions (*Anderson*, 1992, 1993).

Surface-layer stability effects were not found to be significant, lending support to the characterization of the area at the time of the measurements as open ocean. Nor were stability effects apparent when using the more physically rigorous LKB surface-layer model. Stability effects are likely to be important in coastal regions; in light of Blanc's conclusion, investigations need to be undertaken to determine if these effects can be sufficiently characterized.

Range-varying evaporation duct structure was shown to account for differences that had not been previously explained, even though the meteorological data used represented a crude approach to characterizing the variation of the evaporation duct over the path.

This study demonstrates a credible capability for assessment of propagation in the evaporation duct with relatively simple meteorological measurements. The EREPS propagation models yielded results that were comparable to the RPO model in the range-independent mode for this propagation path. *Jeske* (1971) summed up a discussion of propagation in the evaporation duct by stating ". . . the problem of prediction of propagation conditions by the aid of simple meteorological measurements in the lower maritime boundary layer of the open sea is more or less solved." Certainly, in comparison to standard diffraction calculations, the results in figures 16 through 39 support this statement. Progress in the past two decades has been in the development of robust, meteorological, surface-layer models and efficient, high-fidelity, propagation models. With regard to the latter, RPO was executed 13,484 times, not including reruns, on an IBM-compatible PC to construct the predicted propagation loss for comparisons to observations. The speed and efficiency of the hybrid RPO model make comprehensive propagation analyses quite manageable for reporting.

REFERENCES

Anderson, K.D. 1987. "Worldwide Distributions of Shipboard Surface Meteorological Observations for EM Propagation Analysis," NOSC TD 1150 (Sep). Naval Ocean Systems Center, San Diego, CA.

Anderson, K.D. 1990. "94-GHz propagation in the evaporation duct," *IEEE Trans. Antennas Propagat.*, vol. 38, no. 5, pp. 746–753.

Anderson, K.D. 1992. "Remote sensing of the evaporation duct using an x-band radar," *Remote Sensing of the Propagation Environment*, AGARD CP-502, pp. 3–1 to 3–9.

Anderson, K.D. 1993. "Radar Detection of Low-Altitude Targets in a Maritime Environment," NRaD TR 1630 (Nov), vols. 1 & 2, Naval Command, Control and Ocean Surveillance Center RDT&E Division, San Diego, CA.

Blanc, T.V. 1987. "Accuracy of Bulk-Method-Determined Flux, Stability, and Sea Surface Roughness," *J. Geophys. Res.*, vol. 92, no. C4, pp. 3867–3876.

Hitney, H.V. and J.H. Richter. 1976. "Integrated Refractive Effects Prediction System (IREPS)," *Nav. Eng. J.*, vol. 88, no. 2, pp. 257–262.

Hitney, H.V and R. Vieth. 1990. "Statistical assessment of evaporation duct propagation," *IEEE Trans. Antennas Propagat.*, vol. 38, no. 6, pp. 794–799.

Hitney, H.V. and L.R. Hitney. 1990. "Frequency diversity effects of evaporation duct propagation," *IEEE Trans. Antennas Propagat.*, vol. 38, no. 10, pp. 1694–1700.

Hitney, H.V. 1992. "Hybrid ray optics and parabolic equation methods for radar propagation modeling," *RADAR 92*, IEE Conference Publication No. 365 (pp. 58–61), 12–13 Oct. 1992. Brighton, England, U.K.

Jeske, H. 1971. "The State of Radar-Range Prediction over Sea," in *Tropospheric Radio Wave Propagation, Part II*, NATO–AGARD Conference Proceedings No. 70 (pp. 50–1 to 50–10).

Jeske, H. 1973. "State and limits of prediction methods of radar wave propagation conditions over sea," *Modern Topics in Microwave Propagation and Air-Sea Interaction*, A. Zancla, ed., Reidel Pub., pp. 131–148.

Liu, W.G. and T.V. Blanc. 1984. "The Liu, Katsaros, and Businger (1979) bulk atmospheric flux computational iteration program in FORTRAN and BASIC," NRL Memo. Rept. 5291, Naval Research Laboratory, Washington, DC.

Patterson, W.L. 1985. "Comparison of evaporation duct and path loss models," *Radio Sci.*, vol. 20, no. 5, pp. 1061–1068.

Patterson, W.L., C.P. Hattan, H.V. Hitney, R.A. Paulus, A.E. Barrios, G.E. Lindem, and K.D. Anderson. 1990. "Engineer's Refractive Effects Prediction System (EREPS) Revision 2.0," NOSC TD 1342 (Feb), (with revision 2.2 updates), Naval Ocean Systems Center, San Diego, CA.

Paulus, R.A. 1985. "Practical application of an evaporation duct model," *Radio Sci.*, vol. 20, no. 4, pp. 887–896.

Paulus, R.A. 1989a. "Data Quality in EM Propagation Models," *Proceedings: Conference on Microwave Propagation in the Marine Boundary Layer*," NEPRF TR 89–02 (pp. 2–117 to 2–138). January, Naval Environmental Prediction Research Facility, Monterey, CA.

Paulus, R.A. 1989b. "Specification for Environmental Measurements to Assess Radar Sensors," NOSC TD 1685 (Nov), Naval Ocean Systems Center, San Diego, CA.

Richter, J.H. and H.V. Hitney. 1988. "Antenna Heights for the Optimum Utilization of the Oceanic Evaporation Duct," vols. 1 & 2, NOSC TD 1209 (Jan), Naval Ocean Systems Center, San Diego, CA.

APPENDIX A

REPORT

As *Jeske* (1973) noted, negative duct heights (or "anti-duct") may be calculated under certain conditions. The equation (*Paulus*, 1989) for evaporation duct height under stable surface layer conditions is

$$\delta = \frac{\Delta N_p}{b_1 B - \Delta N_p \frac{\alpha}{L'}}, \tag{A-1}$$

where δ is evaporation duct height, ΔN_p is the difference in potential refractivity between the air at some reference height and the sea surface, b_1 is the critical gradient of potential refractivity to cause trapping (taken by Jeske to be $-0.125\ m^{-1}$), B is a positive-valued stability function, α is a positive constant, and L' is the Monin-Obukhov stability length (positive for stable conditions). Normally, ΔN_p is negative; however, in subrefractive conditions, ΔN_p is positive, resulting in a negative evaporation duct height. The physical interpretation of this negative height is that its absolute value is the height where

$$\frac{\partial N_p}{\partial z} = +0.125 m^{-1}, \tag{A-2}$$

or in terms of modified refractivity, M,

$$\frac{\partial M}{\partial z} = +0.26 m^{-1}, \tag{A-3}$$

where subrefraction is conventionally defined as M-gradients exceeding $0.157\ m^{-1}$; thus, using a negative evaporation duct height generates a subrefractive profile.

REPORT DOCUMENTATION PAGE

Form Approved OMB No. 0704-0188

1. AGENCY USE ONLY (Leave blank)	2. REPORT DATE	3. REPORT TYPE AND DATES COVERED
	March 1994	Final: March 1994

4. TITLE AND SUBTITLE

PROPAGATION IN THE EVAPORATION DUCT
Model Predictions and Comparisons to Data

5. FUNDING NUMBERS

6. AUTHOR(S)

R. A. Paulus

7. PERFORMING ORGANIZATION NAME(S) AND ADDRESS(ES)

Naval Command, Control and Ocean Surveillance Center (NCCOSC),
RDT&E Division
San Diego, CA 92152–5001

8. PERFORMING ORGANIZATION REPORT NUMBER

TR 1644

9. SPONSORING/MONITORING AGENCY NAME(S) AND ADDRESS(ES)

Office of Naval Research
800 North Quincy Street (Code 322)
Arlington, VA 22217

10. SPONSORING/MONITORING AGENCY REPORT NUMBER

11. SUPPLEMENTARY NOTES

12a. DISTRIBUTION/AVAILABILITY STATEMENT

Authorized for public release; distribution is unlimited.

12b. DISTRIBUTION CODE

13. ABSTRACT (*Maximum 200 words*)

In 1972, a series of radio propagation measurements in the 1- to 40-GHz frequency range was performed in the eastern Mediterranean. A 35.2-km over-the-horizon propagation path was established between the islands of Naxos and Mykonos in the Aegean Sea. During the November measurement period, surface meteorological measurements were made and used to characterize evaporation ducting conditions on both islands, Ornos Beach on Mykonos and the Greek Weather Service on Naxos. These data have been quantitatively analyzed with the Engineer's Refractive Effects Prediction System (EREPS), the Radio Physical Optics (RPO) propagation model assuming horizontal homogeneity of the evaporation duct as characterized by the Mykonos meteorological data, and RPO utilizing the data at both Mykonos and Naxos to provide range-varying refractive structure. Comparisons of predicted propagation loss by the three approaches to the observed data show the influences of the EREPS single-mode assumption, surface-layer stability, and range-varying evaporation ducting.

14. SUBJECT TERMS

propagation assessment
environmental data
tactical decision aids

15. NUMBER OF PAGES

16. PRICE CODE

17. SECURITY CLASSIFICATION OF REPORT	18. SECURITY CLASSIFICATION OF THIS PAGE	19. SECURITY CLASSIFICATION OF ABSTRACT	20. LIMITATION OF ABSTRACT
UNCLASSIFIED	UNCLASSIFIED	UNCLASSIFIED	SAME AS REPORT

21a. NAME OF RESPONSIBLE INDIVIDUAL	21b. TELEPHONE (Include Area Code)	21c. OFFICE SYMBOL
R. A. Paulus	(619) 553-1424	Code 543

INITIAL DISTRIBUTION

Code 0012	Patent Counsel	(1)
Code 0274	Library	(2)
Code 0275	Archive/Stock	(6)
Code 50	H. O. Porter	(1)
Code 54	J. H. Richter	(1)
Code 543	R. A. Paulus	(25)

Defense Technical Information Center
Alexandria, VA 22304–6145 (4)

NCCOSC Washington Liaison Office
Washington, DC 20363–5100

Center for Naval Analyses
Alexandria, VA 22302–0268

Navy Acquisition, Research and Development
Information Center (NARDIC)
Arlington, VA 22244–5114

GIDEP Operations Center
Corona, CA 91718–8000

Office of Naval Research
Arlington, VA 22217–5000 (2)

Space and Naval Warfare Systems Command
2451 Crystal Drive
Arlington, VA 22245–5200

Naval Surface Warfare Center
Dahlgren Division
Dahlgren, VA 22448–5000

Naval Meteorology and Oceanographic Command
Stennis Space Center, MS 39529–5000

University of Texas at Austin
Applied Research Laboratories
Austin, TX 78713–8029